AIChE WILEY InterScience DISCOVER SOMETHING GREAT

FLUID MECHANICS AND TRANSPORT PHENOMENA

Carbon Xerogels as Catalyst Supports: Study of Mass Transfer

Nathalie Job, Benoît Heinrichs, Stéphanie Lambert, and Jean-Paul Pirard
Laboratoire de Génie Chimique, B6a, Université de Liège, B-4000 Liège, Belgium

Jean-François Colomer
Laboratoire de Résonance Magnétique Nucléaire, Facultés Universitaires Notre-Dame de la Paix, rue de Bruxelles 61, B-5000 Namur, Belgium

Bénédicte Vertruyen
SUPRATECS - Laboratoire de Chimie Inorganique Structurale, B6a, Université de Liège, B-4000 Liège, Belgium

José Marien
Laboratoire de Physicochimie des Surfaces, B6c, Université de Liège, B-4000 Liège, Belgium

DOI 10.1002/aic.10870
Published online May 3, 2006 in Wiley InterScience (www.interscience.wiley.com).

Hydrodechlorination of 1,2-dichloroethane on Pd-Ag alloys was used as a test reaction in order to study mass transfer in carbon xerogel supports. The selected supports were obtained from evaporative drying and pyrolysis of resorcinol-formaldehyde aqueous gels. Since the pore texture of these materials can be tailored through the adequate choice of the gel synthesis conditions, the maximum pore size of the supports was fixed at 10×10^{-9} *m,* 30×10^{-9} *m (mesoporous supports), or* 70×10^{-9} *m (macroporous support). One Pd-Ag/activated carbon catalyst was also prepared for comparison. Diffusional limitations in mesoporous xerogels and in the active charcoal were highlighted by catalytic measurements with pellets of increasing size (*$\leq 1.125 \times 10^{-3}$ *m); the effectiveness factor of the catalyst decreases when the pellet size increases. On the contrary, it remains equal to 1 for the macroporous support, whatever the pellet size, which shows that diffusional limitations can be completely avoided by choosing an appropriate pore size range.* © 2006 American Institute of Chemical Engineers *AIChE J,* 52: 2663–2676, 2006
Keywords: mass transfer, diffusion, carbon xerogel, supported catalysts, tailored texture

Introduction

Since their introduction by Pekala,[1] carbon materials issued from drying and pyrolysis of organic gels have been the subject of many studies,[2] and their use as catalyst support was considered on several occasions.[3] Carbon xerogels are materials obtained from evaporative drying and pyrolysis of organic gels. In particular, resorcinol-formaldehyde aqueous gels lead to carbon materials whose texture can be adjusted within a very wide pore size range by choosing correctly the values of the synthesis variables.[4-9] Exclusively microporous, micro-mesoporous, or micro-macroporous carbons can be produced depending on the pH and the dilution ratio of the starting resorcinol-formaldehyde aqueous solution. When the dilution ratio, that is, the solvent/reactants molar ratio, is fixed at 5.7, gels synthesized with pH values between 5.50 and 6.25 lead to

Correspondence concerning this article should be addressed to N. Job at Nathalie.Job@ulg.ac.be.

Table 1. Textural Parameters of Supports and Catalysts

Sample	S_{BET} ($m^2\ kg^{-1}$) $\pm 5 \times 10^3$	V_{DUB} ($m^3\ kg^{-1}$) $\pm 0.01 \times 10^{-3}$	V_p ($m^3\ kg^{-1}$) $\pm 0.05 \times 10^{-3}$	V_{Hg} ($m^3\ kg^{-1}$) $\pm 0.05 \times 10^{-3}$	V_v ($m^3\ kg^{-1}$) $\pm 0.1 \times 10^{-3}$	$w_{0.max}$ (m) $\pm 5 \times 10^{-9}$	ρ_s ($kg\ m^{-3}$) ± 20	ρ_p ($kg\ m^{-3}$) ± 20	ρ_n ($kg\ m^{-3}$) ± 20	ε_p (−) ± 0.02	ε_n (−) ± 0.02
(a) Before Impregnation											
X-525	640×10^3	0.26×10^{-3}	1.18×10^{-3}	1.72×10^{-3}	2.1×10^{-3}	70×10^{-9}	2210	400	1400	0.72	0.36
X-570	585×10^3	0.25×10^{-3}	1.14×10^{-3}	0.82×10^{-3}	$1.14^b \times 10^{-3}$	30×10^{-9}	2190	630	1420	0.56	0.35
X-625	600×10^3	0.25×10^{-3}	0.41×10^{-3}	—[a]	$0.41^b \times 10^{-3}$	10×10^{-9}	2200	1150	1420	0.19	0.35
NC45	970×10^3	0.40×10^{-3}	0.43×10^{-3}	0.20×10^{-3}	0.6×10^{-3}	—[c]	1950	870	—[c]	0.20	—[c]
(b) After Impregnation											
X-525-C	125×10^3	0.05×10^{-3}	0.87×10^{-3}	1.72×10^{-3}	1.8×10^{-3}	70×10^{-9}	1520[d]	400	1400	0.71	0.07[d]
X-570-C	335×10^3	0.15×10^{-3}	0.95×10^{-3}	0.82×10^{-3}	$0.95^b \times 10^{-3}$	30×10^{-9}	1810[d]	640	1420	0.53	0.21[d]
X-625-C	130×10^3	0.06×10^{-3}	0.23×10^{-3}	—[a]	$0.23^b \times 10^{-3}$	10×10^{-9}	1550[d]	1160	1440	0.19	0.09[d]
NC45-C	810×10^3	0.30×10^{-3}	0.32×10^{-3}	0.20×10^{-3}	0.5×10^{-3}	—[c]	1630[d]	870	—[c]	0.20	—[c]

[a]Not measurable.
[b]$\pm 0.05 \times 10^{-3}\ m^3\ kg^{-1}$ (micro-mesoporous sample whose total pore volume V_v is equal to V_p).
[c]Not pertinent.
[d]The difference observed between the support and the catalyst is due to the blocking of pores by metal particles.

micro-mesoporous carbon materials whose pore volume and maximum pore size increase as the synthesis pH decreases.[5] At pH lower than 5.50, the carbon obtained after evaporative drying and pyrolysis under nitrogen flow at 1073 K is micro- and macroporous and loses its mechanical properties at very low pH. When the pH exceeds 6.50, the material obtained is totally non porous. The pH range leading to micro-mesoporous materials can be shifted to larger or lower values by the presence of additives.[6,10] The drying step can also be performed by convective air-drying,[7,8] which makes the process simple and feasible at the industrial scale. The porous carbon materials can be designed as monoliths of various shapes, pellets, or powder.

The ability to control at will the pore size in carbon xerogels is certainly an advantage compared to classical active charcoals, whose textural parameters are mainly fixed by the origin of the raw material. Indeed, active charcoals are produced from the pyrolysis of natural sources like wood, coal, nutshells, or fruit pits, and the pore texture obtained after thermal treatment strongly depends on the nature of the precursor. This can lead to reproducibility problems in terms of pore texture, surface properties, and even chemical composition; one of the problems of using carbons derived from agricultural by-products is the variability in feedstock, resulting in limited control over pore sizes and volumes. Moreover, active charcoals are generally microporous, with low macropore or mesopore volumes,[11] which often induces diffusional limitations during catalytic processes. On the contrary, the presence of large amounts of meso- or macropores should minimize diffusion limitations inside carbon supports synthesized by the sol-gel process, and these supports could be designed according to the considered reaction. In addition, these carbon materials possess a very good mechanical strength and monoliths of various shapes can be easily produced.

The aim of this article is to study mass transfer inside carbon xerogels during a well-known chemical reaction and to show that it is possible to completely eliminate diffusional limitations inside the catalyst pellets provided that the carbon xerogel texture is adequately adjusted through an appropriate choice of synthesis variables values. Indeed, the texture control of the carbon xerogel via the synthesis variables of the resorcinol-formaldehyde gel enables us to choose the carbon texture precisely. In a previous study,[12] a micro-mesoporous carbon xerogel was used as support for Pd-Ag catalysts designed for chlorinated alkanes hydrodechlorination reactions. These catalysts were prepared by wet impregnation with a solution containing metal nitrates, water, and nitric acid. Pd-Ag/carbon xerogel catalysts proved to be efficient for the selective hydrodechlorination of 1,2-dichloroethane into ethylene when the global Ag content was equal to 1.5 wt.% or higher, the Pd content being fixed at 1.5 wt.%. The same reaction-catalyst pair was chosen to study mass transfer in carbon xerogels supported catalysts.

Experimental Procedures

Synthesis of Pd-Ag catalysts supported on carbon xerogels and activated charcoal

The synthesis process of carbon xerogels was extensively described elsewhere.[5] The selected supports for Pd-Ag/carbon xerogel catalysts were obtained from evaporative drying and pyrolysis of three aqueous resorcinol-formaldehyde gels with fixed dilution ratio (solvent/reactants molar ratio = 5.7) and resorcinol/formaldehyde molar ratio ($R/F = 0.5$), and three different starting pH values. The pH was fixed at 5.25, 5.70, and 6.25, respectively, with NaOH solutions. The aqueous gels obtained after gelation and aging during 72 h at 358 K were then dried by vacuum evaporation without any pre-treatment. After drying, the gels were pyrolyzed at 1073 K under nitrogen flow in a tubular oven. The fourth support chosen was an activated carbon, CECA Acticarb NC45. The pore texture of the carbon supports was deduced from the analysis of the nitrogen adsorption-desorption isotherms and from mercury porosimetry. The main texture parameters are listed in Table 1 and discussed below.

The supports were crushed and sieved between 1.250×10^{-3} and 1.000×10^{-3} m. The pellets were then impregnated by immersion in aqueous nitric acid solutions containing various amounts of $AgNO_3$ and $Pd(NO_3)_2.H_2O$. The previous study conducted on carbon xerogels as Pd-Ag catalysts supports[12] showed that, while Pd and Ag can form solid solutions in any proportion, the Ag atomic content in the alloy particles is limited to about 50%; the Ag in excess is deposited on the carbon surface as pure Ag particles that quickly become inactive during the hydrodechlorination reaction due to the formation of AgCl.[13] The metal concentrations of the various im-

Table 2. Solutions Composition

	Solution Composition			
Catalyst	HNO_3[a] (cm^3)	H_2O (cm^3)	$Pd(NO_3)_2 \cdot H_2O$ (g)	$AgNO_3$ (g)
X-525-C	7.7	2.3	0.1564	0.1138
X-570-C	7.7	2.3	0.2706	0.1969
X-625-C	7.7	2.3	0.7845	0.5706
NC45-C	7.7	2.3	0.7642	0.5558

[a]Solution 69% in water.

pregnating solutions were thus calculated so that the nominal content was equal to 1.5 wt.% for both metals. Four $AgNO_3$ aqueous solutions and four $Pd(NO_3)_2.H_2O$ in nitric acid solutions with various metal salts concentrations were first prepared. Then 7.7 cm^3 from each solution containing $Pd(NO_3)_2.H_2O$ in aqueous nitric acid (69 wt.%) was added to 2.3 cm^3 of the corresponding $AgNO_3$ aqueous solution. The final composition of an impregnation solution devoted to the corresponding support is reported in Table 2. Carbon pellets (4 g) were immersed in the corresponding solution for 24 h. The samples were then filtered in order to remove the excess of solution and dried under flowing air at ambient temperature for 24 h. The drying process was completed by vacuum drying (24 h, 423 K). After drying, a small part of each sample to be used for characterization was reduced for 3 h in flowing H_2 at 623 K (H_2 flowrate: 0.025 mmol s^{-1}, heating rate from room temperature to 623 K: 350 K h^{-1}). The main part was crushed again and sieved in order to obtain four samples of each catalyst with decreasing mean pellet size. The meshes of the sieves were 1.250, 1.000, 0.710, 0.500, and 0.250×10^{-3} m wide.

Samples designation

The supports are denominated as follows throughout the article: for carbon xerogels, the letter X is followed by the pH, multiplied by 100, of the precursors solution of the original gel; the active charcoal is referenced as NC45. A C is added to distinguish the final Pd-Ag catalyst, and the lowest of the two mesh widths is given at the end when needed. For example, X-625 is the carbon support issued from drying and pyrolysis of a resorcinol-formaldehyde gel synthesized at pH = 6.25, and X-625-C-250 is the corresponding Pd-Ag catalyst after impregnation, drying, and reduction treatments, crushed and sieved between 0.250 and 0.500×10^{-3} m. In the case of X-625-C, a fifth sample corresponding to powder (pellet size $< 0.250 \times 10^{-3}$ m) was also tested. This particular sample is referred to as X-625-Cp.

Sample characterization

The pore texture of supports before impregnation as well as Pd-Ag/C catalysts was characterized by the analysis of nitrogen adsorption-desorption isotherms performed at 77 K with a Sorptomatic Carlo Erba 1900 instrument. The analysis of the isotherms was performed according to the methodology proposed by Lecloux[14] and provided the BET specific surface area, S_{BET}, the micropore volume calculated by the Dubinin-Radushkevich equation, V_{DUB}, and the pore volume calculated from the adsorbed volume at saturation, V_p. The maximum pore width, $w_{0,max}$, that is, the pore width limit under which smaller pores represent 95% of the total pore volume, was deduced from pore size distributions provided by the Broekhoff-de Boer method[14] in the case of micro-mesoporous carbon xerogels. The Broekhoff-de Boer method was applied to the adsorption branch of the isotherm. In the case of samples containing macropores (X-5.75, NC45, and the corresponding catalysts), mercury porosimetry was used to measure the pore volume corresponding to pores larger than 7.5×10^{-9} m. Indeed, the pore volume calculated from the adsorbed volume at saturation is very imprecise or incomplete when the solid contains macropores (pores larger than 50×10^{-9} m). In this case, the total void volume V_v is calculated from the combination of nitrogen adsorption-desorption and mercury porosimetry measurements[15] (Eq. 1):

$$V_v = V_{DUB} + V_{cum<7.5nm} + V_{Hg} \quad (1)$$

where V_{DUB} takes into account pores of width lower than 2×10^{-9} m (micropores), V_{Hg} is the specific pore volume measured by mercury porosimetry, and $V_{cum<7.5nm}$ is the cumulative volume of pores of width between 2×10^{-9} m and 7.5×10^{-9} m determined by the Broekhoff-de Boer theory. Moreover, since intrusion without crushing occurs when the carbon materials chosen are submitted to mercury porosimetry, the pore size distribution of pores larger than 7.5×10^{-9} m and $w_{0,max}$ were deduced from the Washburn theory[16,17] (applied to the intrusion of mercury with increasing pressures). For standardization reasons, the pore volumes and specific surface areas are expressed in $m^3\ kg^{-1}$ and $m^2\ kg^{-1}$, respectively, and not in $cm^3\ g^{-1}$ and $m^2\ g^{-1}$ as usual.

The bulk density of the pellets, ρ_p, was measured by mercury pycnometry, and the skeletal density, ρ_s, was obtained from helium pycnometry measurements. Again, these parameters were measured before and after impregnation.

Actual metal contents were determined by inductively coupled plasma-atomic emission spectroscopy (ICP-AES). Metal particles were examined by X-ray diffraction (XRD), transmission electron micrography (TEM), and CO chemisorption.[18,19] Details about the specific procedures used can be found elsewhere[12]; the combination of these three techniques enabled us to obtain the metal particles size as well as their bulk and surface composition.[20]

Catalytic tests

The 1,2-dichloroethane consumption rate was measured with each catalyst at 473, 523, 573, and 623 K and at 0.3 MPa. Each temperature step lasted 3 h; then the temperature was decreased to 573 K again and data were collected for 5 more hours. The measurements were repeated with the four pellet sizes for every catalyst.

The feeding section of the kinetic measurement device was constituted of two gas lines for H_2 and He, whose flowrates were adjusted with Brooks mass flowrate controllers. 1,2-dichloroethane was supplied in liquid phase with a Gilson piston pump. A loop located in the oven upstream from the reactor ensured the vaporization of $CH_2Cl\text{-}CH_2Cl$. The stainless steel tubular reactor with an internal diameter of 10^{-2} m and a length of 0.2 m was placed in a convection oven whose temperature was controlled and programmed. The temperature within the reactor was measured with a thermocouple slipped in a stainless steel sheath immersed in the catalyst bed. A pressure controller operating a compressed air valve located

downstream from the reactor regulated the total pressure. Feed gas flows were kept constant by mass flow controllers: 0.459 mmol s^{-1} helium and 0.025 mmol s^{-1} hydrogen. The 1,2-dichloroethane flow was equal to 0.012 mmol s^{-1}. These conditions ensure that no external mass transfer limitations occur.[21]

The catalytic bed was constituted of 0.2×10^{-3} kg of non-reduced Pd-Ag/C catalyst pellets. Prior to the measurement, the catalyst was reduced in situ; under flowing hydrogen (0.025 mmol s^{-1}) and at a pressure of 0.125 MPa, the catalyst was heated from room temperature to 623 K at a rate of 350 K h^{-1} and was maintained at 623 K for 3 h.

The effluent of the reactor was analyzed by gas chromatography with a flame ionization detector (FID). Although this analysis method theoretically enabled us to measure 1,2-dichloroethane, ethylene, and ethane concentrations, only C_2H_4 and C_2H_6 concentrations were used in this study due to the too large imprecision of $CH_2Cl\text{-}CH_2Cl$ concentration measurements; indeed, since 1,2-dichloroethane is liquid at room temperature, condensation could occur in the pipes before injection in the FID device.

Results

Catalysts characterization

The nitrogen adsorption-desorption isotherms corresponding to the raw supports and to the final catalysts after impregnation, drying, and reduction treatments are shown in Figures 1a and 1b, respectively. The raw supports X-625 and X-570 are micro-mesoporous (combination of type I and type IV isotherms), whereas X-525 is micro-macroporous (combination of type I and type II isotherms). The active charcoal NC45 displays a type I isotherm (microporous solid) with a very small hysteresis corresponding to a few mesopores (type IV isotherm). The textural parameters of the supports before metal deposition are reported in Table 1. The specific surface area and the micropores volume are very similar for the three carbon xerogels (S_{BET} ranging from 585×10^3 to 640×10^3 m^2 kg^{-1}; V_{DUB} equal to 0.25×10^{-3} or 0.26×10^{-3} m^3 kg^{-1}), but their total pore volume strongly depends on the starting pH, as expected; the total pore volume V_v ranges from 2.1×10^{-3} (X-525) to 0.41×10^{-3} m^3 kg^{-1} (X-625). In parallel, the xerogel bulk density increases with the starting pH of the precursors solution. The skeletal density remains constant and equal to about 2200 kg m^{-3}, which is slightly below the density of graphite (2250 kg m^{-3}). The active charcoal contains more micropores than the carbon xerogels ($S_{BET} = 970 \times 10^3$ m^2 kg^{-1}; $V_{DUB} = 0.40 \times 10^{-3}$ m^3 kg^{-1}), and some macroporosity is also detected by mercury porosimetry ($V_v = 0.6 \times 10^{-3}$ m^3 kg^{-1}). Its bulk and skeletal densities are 870 and 1950 kg m^{-3}, respectively.

The meso- and macropore size distributions of the three carbon xerogel supports are shown on Figure 2a. Their maximal pore sizes, $w_{0,max}$, that is, the pore width limit under which smaller pores represent 95% of the total pore volume, are 10×10^{-9} m (X-625), 30×10^{-9} m (X-570), and 70×10^{-9} m (X-525). Neither larger pores nor cracks were detected by mercury porosimetry. In the case of the active charcoal NC45, the pore size distribution is much broader (Figure 2b); pore size ranges from 10×10^{-9} m to 4×10^{-6} m, although the pore volume corresponding to meso and macropores is rather low

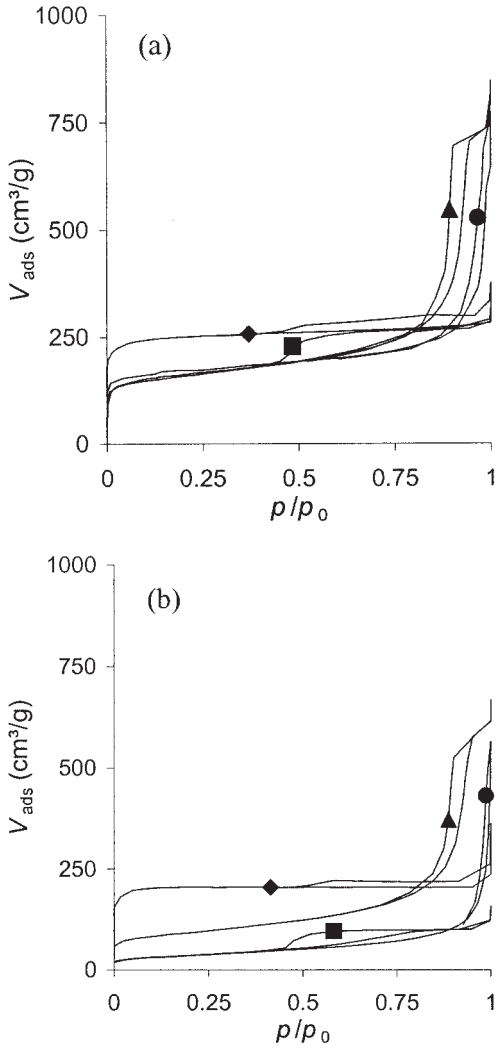

Figure 1. Nitrogen adsorption-desorption isotherms (a) of the raw supports and (b) of the corresponding catalysts after impregnation.

Xerogels X-525 (●), X-570 (▲), X-625 (■), and active charcoal NC-45 (◆).

(0.2×10^{-3} m^3 kg^{-1}). The active charcoal NC45 is in fact less homogeneous than carbon xerogels, and the largest pores can be regarded as microfissures in the carbon material.

As a general comment, the specific surface area and skeletal density decreases after impregnation (Table 1). The meso- or macropore volumes, V_{Hg}, are not affected, whatever the support. In order to determine if the micropore volume decrease is due either to the acidic treatment or to the metal deposit, carbon xerogels supports and the active charcoal NC45 were immersed in nitric acid aqueous solution similar to that used for metal impregnation but without any metal salt. After drying, the samples were examined by nitrogen adsorption-desorption. Measurements show that, in all cases, no micropore volume change occurs when no metal salt is present. Since such a treatment does not affect the texture of the support, it was concluded that micropores are blocked by metal particles in the final catalysts.

Table 3 collects results obtained from ICP, XRD, TEM, and

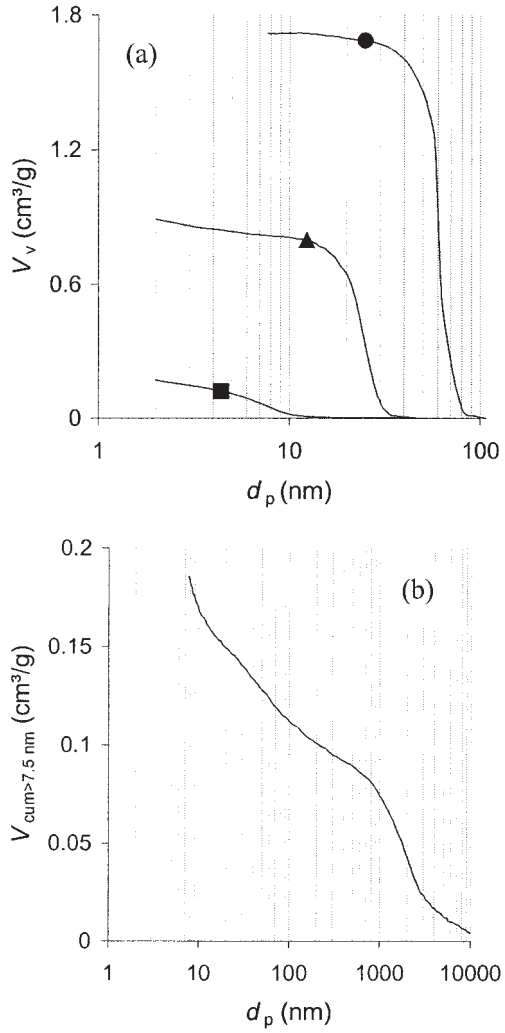

Figure 2. Meso- and macropore size distribution.

(a) Carbon xerogels X-525 (●), X-570 (▲), and X-625 (■). (b) Active charcoal NC45.

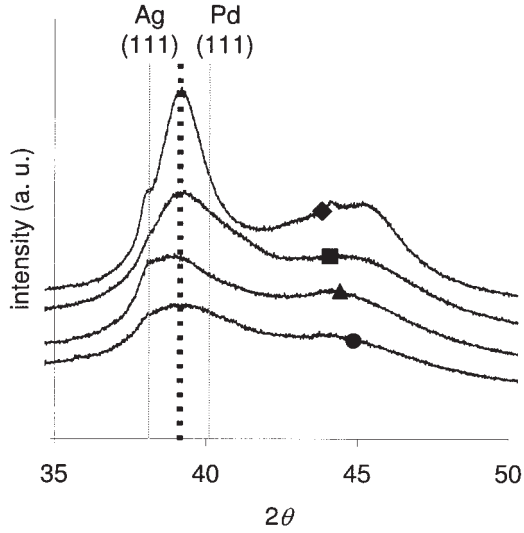

Figure 3. X-ray diffractograms.

X-525-C (●), X-570-C (▲), X-625-C (■), and NC45-C (♦). The diffractograms were shifted from each other to avoid curves superposition, and therefore no intensity scale other than "arbitrary units" (a.u.) is mentioned.

CO chemisorption. The results are very similar to those obtained previously in the case of xerogels supports.[12]

ICP measurements show that the metal loading is in each catalyst larger than the expected value (1.5 wt.%)—from 2.0 to 3.2 wt.% in the case of Pd, and from 1.5 to 2.2 wt.% in the case of Ag. This suggests that some metal cations are adsorbed at the carbon surface. The deviation is larger in the case of carbon xerogels. This could be due to larger interactions between the xerogels and the metal ions and to the fact that the diffusion of the impregnation solution is easier in the carbon xerogels than in the active charcoal.

Whatever the support, the X-ray diffractogram (Figure 3) exhibits a broad peak located between the (111) Bragg lines of pure Pd and pure Ag; this indicates the presence of small alloy particles. The fraction of Pd atoms in the bulk of the alloy particles, x_{Pd} (Table 3), can be deduced from the alloy peak position.[22] Assuming that all the bimetallic particles have the same Pd-Ag composition in the considered catalyst, their mean size (d_{XRD}) can be calculated from the peak broadening after deconvolution and Scherrer's formula.[19] The Pd content of the alloy particles ranges from 54 to 62 at.%, which is not significantly different and slightly higher than previous results.[12] The size of the alloy particles, d_{XRD}, is almost constant (3.5 to 4.2 nm) for all xerogel supports, but increases in the case of the activated charcoal (5.8 nm). Pure silver particles are also detected by the presence of a shoulder whose position corre-

Table 3. Results from ICP, XRD, TEM, and CO Chemisorption

	ICP			XRD			TEM					CO		
Catalyst	Pd_{ICP} (wt. %)	Ag_{ICP} (wt. %)	$[Pd/(Pd + Ag)]_{ICP}$ (at. %)	x_{Pd} (at. %)	d_{XRD} (nm)	$d_{Ag\text{-}XRD}$ (nm)	d_{TEM} (nm)	σ (nm)	d_s (nm)	d_v (nm)	$D_{Pd\text{-}Ag}$ (%)	$n_{s,m}$ (mmol g_{Pd}^{-1})	D_{Pd} (%)	x_{Pd_s} (at. %)
X-525-C	2.3	2.2	52	59	3.5	10.2	3.1	0.94	3.4	3.7	33	0.652	7	12
X-570-C	2.6	1.9	57	54	3.6	12.3	3.2	0.95	3.4	3.6	33	0.586	6	10
X-625-C	3.2	2.1	60	62	4.2	10.2	3.8	0.89	4.0	4.3	28	0.462	5	11
NC45-C	2.0	1.5	57	62	5.8	14.6	4.8	1.42	5.5	5.9	20	0.282	3	9

Pd_{ICP}, Ag_{ICP} = Pd and Ag contents in the catalyst measured by ICP-AES; $[Pd/(Pd + Ag)]_{ICP}$ = fraction of Pd atoms in the whole catalyst obtained from ICP measurements; x_{Pd} = fraction of Pd atoms in the bulk of Pd-Ag alloy particles estimated from XRD; d_{XRD} = mean size of Pd-Ag particles estimated from X-ray line broadening; $d_{Ag\text{-}XRD}$ = mean size of pure Ag particles estimated from X-ray line broadening; d_{TEM} = mean alloy particles sizes estimated from TEM; σ = standard deviations associated with d_{TEM}; d_s = mean surface diameter of Pd-Ag alloy particles, estimated from TEM; d_v = mean volume diameter of alloy particles, estimated from TEM; $D_{Pd\text{-}Ag}$ = overall dispersion of Pd-Ag alloy estimated from TEM; $n_{s,m}$ = amount of CO needed to form a chemisorbed monolayer on surface Pd atoms; D_{Pd} = Pd dispersion estimated from CO chemisorption; x_{Pd_s} = fraction of Pd atoms present at the surface of Pd-Ag alloy particles estimated from the combination of CO chemisorption, XRD, and TEM results.

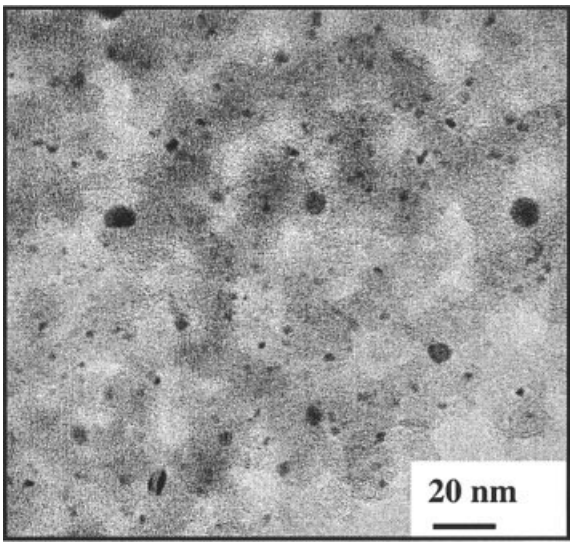

Figure 4. Transmission electron microscopy of Sample X-570-C.

sponds to the (111) Bragg line of Ag. The Ag particles size ($d_{Ag\text{-}XRD}$) is calculated from the deconvoluted curves and ranges from 10.2 to 14.6 nm.

It was previously shown that the metal particle size distribution of Pd-Ag xerogel supported catalysts prepared by impregnation is bimodal, and that the smallest particles family corresponds to Pd-Ag alloy.[12] In this previous study, it was also shown from comparison between TEM and XRD measurements that alloy particles are not larger than 7 nm whereas pure silver particles are 7 to 15 nm in diameter. The results are the same here. An example of a TEM micrograph is shown in Figure 4 (X-570-C); a few large particles (10-15 nm) accompany the many small ones (3-4 nm). Transmission electron microscopy enabled us to measure the alloy particles size. The mean alloy particle size, d_{TEM}, and its respective standard deviation, σ, were calculated for each sample from a set of 60 particles so that the data set was statistically significant. Since they very likely correspond to pure silver, particles larger than 7 nm were excluded from the data set. The alloy particle size distribution is wider in the case of NC45-C: $\sigma = 1.42$ nm instead of 0.89-0.95 nm in the case of xerogel-like supports. The mean volume diameter of the alloy particles, $d_v = \sum n_i d_i^4 / \sum n_i d_i^3$, where n_i is the number of metal particles with a diameter equal to d_i, was calculated from TEM micrographs for comparison with XRD data. Indeed, XRD is sensitive to the volume of particles, and the mean crystallite size calculated from the peak broadening corresponds to a volume weighted average diameter d_v[19]. The values obtained from TEM and XRD are very similar; the maximal difference between d_{XRD} and d_v is 0.2 nm, which confirms that small metal particles observed by TEM correspond to alloy particles.

The mean surface diameter of Pd-Ag alloy particles, $d_s = \sum n_i d_i^3 / \sum n_i d_i^2$, was also evaluated in order to calculate the overall alloy dispersion, that is, the ratio between the number of surface metal atoms of the Pd-Ag alloy particles and the total number of metal atoms in these particles. The alloy dispersion is given by[19]:

$$D_{Pd\text{-}Ag} = \frac{6(v_m/a_m)}{d_s} \quad (2)$$

where v_m is the mean volume occupied by a metal atom in the bulk of the alloy and a_m is the mean surface area occupied by a surface metal atom. Since the metal particles are Pd-Ag alloy, v_m and a_m are arithmetic means of values obtained for Pd and Ag,[19] that is, $v_m = 0.01588$ nm^3 and $a_m = 0.0834$ nm^2. It must be specified that Eq. 2 is applied to alloy particles only. d_s does then correspond to the mean surface diameter of the alloy particles, pure Ag particles being excluded from the data set. Values obtained for $D_{Pd\text{-}Ag}$ are listed in Table 3. The overall alloy dispersion is a bit higher in the case of carbon xerogel supports ($D_{Pd\text{-}Ag}$ ranging from 28 to 33%) than in the case of the active charcoal (20%).

Since CO chemisorption occurs on palladium only,[20,23] it provides a measurement of the palladium dispersion, and more specifically an estimation of the Pd coverage of the alloy surface; indeed, due to the lower surface free enthalpy of Ag in comparison with Pd,[20] the Pd-Ag alloy surface tends to get enriched in silver atoms and the surface composition differs from the bulk composition. The fraction of palladium atoms at the surface, x_{Pd_s}, was deduced from a combination of CO chemisorption results with data coming from XRD and TEM[20]:

$$x_{Pd_s} = D_{Pd} x_{Pd} \frac{1}{D_{Pd\text{-}Ag}} \quad \text{with} \quad D_{Pd} = n_{s,m} M_{Pd} X_{Pd\text{-}CO} \times 10^{-3} \quad (3)$$

where x_{Pd_s} is the fraction of palladium atoms at the surface, D_{Pd} is the Pd dispersion estimated from CO chemisorption, x_{Pd} is the fraction of Pd atoms in the alloy bulk, $D_{Pd\text{-}Ag}$ is the overall alloy dispersion with no distinction between the two metals, $n_{s,m}$ is the amount of CO needed to form a chemisorbed monolayer on palladium sites (mmol g_{Pd}^{-1}), M_{Pd} is the atomic weight of palladium (106.42 g mol^{-1}), and $X_{Pd\text{-}CO}$ is the chemisorption mean stoichiometry, that is, the mean number of Pd atoms on which one CO molecule is adsorbed. Soma-Noto and Sachtler[23] demonstrated that $X_{Pd\text{-}CO} = 1$ (linear bonding) beyond 25 at.% of silver in the bulk of the alloy, which is the case for all the catalysts examined here. Values of D_{Pd} and x_{Pd_s} are given in Table 3. A comparison between bulk (x_{Pd}) and surface (x_{Pd_s}) compositions confirms the surface enrichment with silver; the bulk palladium content is 54 to 62 at.% whereas the fraction of palladium atoms at the surface, x_{Pd_s}, ranges from 9 to 12 at.% only. Note that, since some micropores are blocked by metal, some alloy particles are not fully accessible, which might induce errors on the surface composition calculation. Indeed, if a fraction of the alloy surface is inaccessible, the CO chemisorption does not occur on the whole alloy particle surface, and the fraction of palladium at the alloy surface, x_{Pd_s}, is underestimated. Nevertheless, the surface compositions obtained are in good agreement with previous studies. According to previous results,[20] Pd-Ag alloy particles with a Pd bulk content x_{Pd} near 60 at.%. can display Pd surface contents ranging from 5 to 15 at.%.

As a general conclusion, the metal particles are very similar in terms of bulk and surface composition, whatever the support chosen. The only difference is the Pd-Ag alloy particles size, which is larger in the case of active charcoal supported cata-

Table 4. Catalytic Tests Results

Catalyst	Conversion (%)		C_2H_4 Selectivity (%)		r_1 (mmol kg^{-1} s^{-1})		η (−)		Φ_p (−)		Φ_n (−)	
	573 K	623 K	573 K	623 K	573 K	623 K	573 K	623 K	573 K	623 K	573 K	623 K
X-525-C-1000	12.1	34.5	98.9	99.2	8.6	21.3	1.00	1.00	0.021	0.066	4×10^{-6}	1×10^{-5}
X-525-C-710	12.2	34.6	98.9	99.2	8.5	21.1	1.00	0.99	0.011	0.031	4×10^{-6}	1×10^{-5}
X-525-C-500	12.1	34.2	98.9	99.2	8.5	21.0	1.00	0.99	0.005	0.015	4×10^{-6}	1×10^{-5}
X-525-C-250	12.1	34.3	98.9	99.2	8.5[b]	21.3[b]	1.00	1.00	0.001	0.004	4×10^{-6}	1×10^{-5}
X-570-C-1000	18.7	45.3	95.5	97.1	12.0	28.2	0.83	0.84	0.19	0.55	6×10^{-8}	2×10^{-7}
X-570-C-710	19.6	51.4	96.9	97.8	12.8	31.7	0.88	0.95	0.11	0.33	6×10^{-8}	2×10^{-7}
X-570-C-500	21.2	53.7	95.7	97.3	14.3	33.3	0.98	1.00	0.06	0.17	7×10^{-8}	2×10^{-7}
X-570-C-250	21.3	55.0	95.9	97.2	14.5[b]	33.5[b]	1.00	1.00	0.015	0.04	7×10^{-8}	2×10^{-7}
X-625-C-1000	5.6	12.6	71.8	81.6	3.5	7.8	0.47	0.40	2.2	5.3	8×10^{-9}	2×10^{-8}
X-625-C-710	6.7	15.4	78.3	86.3	4.2	9.6	0.55	0.49	1.3	3.4	1×10^{-8}	3×10^{-8}
X-625-C-500	8.7	19.9	81.7	87.8	5.4	12.4	0.72	0.63	0.9	2.2	1×10^{-8}	4×10^{-8}
X-625-C-250	12.2	27.8	84.3	87.8	6.9	17.2	0.91	0.88	0.3	0.8	2×10^{-8}	6×10^{-8}
X-625-Cp	12.5	31.7	95.4	96.6	7.6[b]	19.6[b]	1.00	1.00	0.1	0.34	2×10^{-8}	7×10^{-8}
NC45-C-1000	5.6	18.0[a]	98.3	98.5	3.6	11.0	0.64	0.68	—[c]	—[c]	—[c]	—[c]
NC45-C-710	5.6	18.0[a]	98.8	98.9	3.5	11.1	0.67	0.68	—[c]	—[c]	—[c]	—[c]
NC45-C-500	6.3	20.0[a]	98.3	98.4	3.9	12.2	0.73	0.75	—[c]	—[c]	—[c]	—[c]
NC45-C-250	8.7	26.8[a]	98.3	98.5	5.4[b]	16.2[b]	1.00	1.00	—[c]	—[c]	—[c]	—[c]

r_1: apparent reaction rate; η: effectiveness factor; Φ_p: Weisz modulus at the pellet level; Φ_n: Weisz modulus at the nodule level.
[a]Imprecise due to deactivation.
[b]Considered as equal to the intrinsic reaction rate.
[c]Not calculable with the two-level model.

lysts (about 5-6 nm instead of 3-4 nm). The metal loading is also slightly higher in the case of carbon xerogels, the deviation from the nominal value (1.5 wt.% in both metals) being larger for Pd.

Catalytic tests

All catalysts produce ethane and ethylene only. Traces of chloroethane or vinylchloride are sometimes observed, but can be considered as negligible (<0.1% of the total conversion). The hydrodechlorination of 1,2-dichloroethane into ethylene and the hydrogenation of ethylene into ethane are two successive reactions, as described by Eqs. 4 and 5. The mechanism will be discussed below.

$$CH_2Cl - CH_2Cl + H_2 \xrightarrow{r_1} CH_2 = CH_2 + 2HCl \qquad (4)$$

$$CH_2 = CH_2 + H_2 \xrightarrow{r_2} CH_3 - CH_3 \qquad (5)$$

The mean values of conversion and ethylene selectivity at 573 and 623 K are regrouped in Table 4 for each catalyst as a function of the pellet size. Since the catalysts generally do not reach stability at 473 and 523 K after 3 and 6 h, respectively, results obtained during these temperature steps were not considered for further calculation. For reasons of catalyst stability, the data given at 573 K are those obtained after the step at 623 K, when going down to 573 K again.

The raw results of the catalytic tests are presented in Figures 5a and 5b for catalysts X-525-C and X-625-C with various mean pellet sizes. The total 1,2-dichloroethane conversion (that is, into ethane or ethylene without distinction) and the ethylene selectivity (that is, the ratio between the amount of ethylene produced and that of 1,2-dichloroethane consumed) are reported as a function of time and temperature. The behaviors of

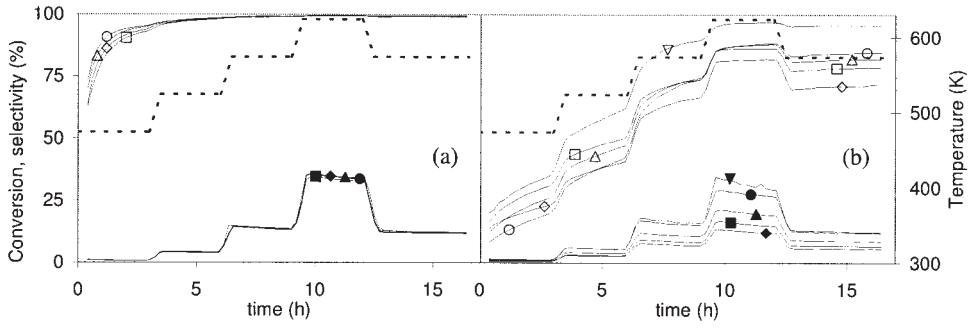

Figure 5. Catalytic tests for samples X-525-C (a) and X-625-C (b).

The dotted black line represents the temperature program. Plain symbols: conversion; empty symbols: ethylene selectivity. Catalysts crushed between 1250 and 1000 μm (◆ and ◇), 710 and 1000 μm (■ and □), 500 and 710 μm (▲ and △), 250 and 500 μm (● and ○), and below 250 μm (▼ and ▽).

catalysts X-525-C and X-625-C are very different from each other. Whatever the temperature, conversion and selectivity are completely independent of the pellet size in the case of X-525-C; all the conversion curves are superimposed (mean conversion: 473 K: 0.8%; 523 K: 4.1%; 573 K: 12.1%; 623 K: 34.5%). On the contrary, for catalyst X-625-C, the 1,2-dichloroethane conversion decreases when the pellet size increases, at every temperature. The difference between the samples is particularly marked at 623 K: the conversion decreases from 27.8% to 12.6% as the mean pellet size increases in the same range. When crushed and sieved below 0.250×10^{-3} m (sample X-625-Cp), the conversion increases up to 31.7% at 623 K. In both catalysts, the 1,2-dichloroethane conversion increases with temperature, but decreases a little with time, which indicates a slight deactivation. The experiment did not last long enough to reach complete stability. Selectivity of X-525-C is very high and independent of the pellet size: 98.9% at 573 K and 99.2% at 623 K. In the case of X-625-C, the catalyst selectivity is much lower and increases with time at 473, 523, and 573 K (Figure 5b). The four curves reach a plateau at 623 K, and the selectivity seems to stabilize by going down again at 573 K. Moreover, the pellet size also plays a role since selectivity decreases at every temperature when the pellet size increases. For example, at 623 K, ethylene selectivity reaches 96.6% for X-625-Cp, but decreases to about 81.6% in the case of X-625-C-1000.

Catalyst X-570-C displays an intermediate behavior. Differences between samples of various pellet size are observed at high temperature (573 and 623 K) and in the case of the largest pellets only ($1.000\text{-}1.250 \times 10^{-3}$ m and $0.710\text{-}0.1000 \times 10^{-3}$ m). At 573 K, conversion decreases from 21.2% to 18.7% when the pellet size increases from $0.500\text{-}0.710 \times 10^{-3}$ m to $1.000\text{-}1.250 \times 10^{-3}$ m. At 623 K, the conversion difference is particularly perceptible between $0.710\text{-}1.000 \times 10^{-3}$ m and $1.000\text{-}1.250 \times 10^{-3}$ m (51.4 and 45.3%, respectively), but the decrease is already noticeable for smaller pellets (X-570-C-250: 55.0%; X-570-C-500: 53.7%).

Conversions obtained with catalyst NC45-C are in most cases lower than those of xerogel supported catalysts with the same pellet size, whatever the texture. The only exceptions are measurements at 623 K with the largest pellets: the conversion is higher than in the case of X-625-C. However, it must be noted that NC45-C deactivates more quickly than the other catalysts at 623 K (5% conversion decrease after 3 h), and that the values of conversion given in Table 4 in these conditions are not stable at the end of the temperature step. Results obtained with the three largest pellet sizes are very similar: the conversion ranges from 5.6 to 6.3% at 573 K and from 18.0 to 20.0% at 623 K. NC45-C-250 is a little more active (8.7% at 573 K; 26.8% at 623 K). Ethylene selectivity is high in all cases (about 98%, whatever the pellet size at 573 and 623 K).

Since the measurement of $CH_2Cl\text{-}CH_2Cl$ concentration in the effluent is imprecise, the apparent hydrodechlorination reaction rate r_1, that is, the apparent rate of 1,2-dichloroethane consumption per unit mass of catalyst, was calculated from the ethane and ethylene concentrations at the reactor outlet (Table 4). The reaction rates obtained are used below in order to calculate the effectiveness factor and the Weisz modulus of the catalysts.

Discussion

Mass transfer in porous catalyst supports has been studied for many years and constitutes a question of the highest importance in chemical engineering.[24-30] In order to study mass transfer inside a porous catalyst, the catalyst pellet is often regarded as a pseudo-continuum, that is, a pseudo-homogeneous medium in which the diffusion of a chemical species is described by the same single effective diffusion coefficient.[24] The diffusion is modeled by Fick's law, the whole pellet being regarded as a homogeneous phase, but in which the fluid molecular diffusivity, D_m, is replaced by the effective diffusivity,[24] D_e. This concept implies that D_e is the same everywhere in the pellet and that the considered length scale for mass transfer is the pellet size. D_e depends on the catalyst support morphology, and more particularly on the void fraction and on the tortuosity factor, which characterizes the tortuous nature of the pores and their constrictions. Moreover, the pore size may have an effect on D_e when smaller than about 100×10^{-9} m; below this limit, the Knudsen diffusion becomes significant with regard to ordinary gas molecular diffusion.[24,25]

Carbon xerogels are composed of spherical-like interconnected carbon nodules whose size can vary from a few nanometers to a few micrometers.[2,9] The nodules size obtained after drying and pyrolysis of the wet gel increases when the starting pH of the precursors solution decreases, leading to larger voids between the nodules.[2,5] The carbon nodules are microporous after pyrolysis, and the voids between the nodules correspond to mesopores and macropores. This morphology does not allow the use of the pseudo-homogeneous concept for the whole pellet. In a previous study,[21,31] Heinrichs et al. developed a model composed of three discrete levels with decreasing sizes in order to describe diffusion in silica xerogels. These levels correspond to: (i) the macroscopic pellet, (ii) an aggregate of silica particles, and (iii) an elementary silica particle. Each level is assumed to be a pseudo-homogeneous medium with its own size, bulk density, void fraction, tortuosity, and single pore width. Since the morphology of carbon xerogels is very close to that of silica xerogels, one could then consider a hierarchical texture composed of two distinct length scales: a first one corresponding to the pellet itself, and a second one corresponding to the microporous carbon nodules. Transmission electron micrographs do not clearly show particle aggregates, and this level was then suppressed from the original model. At the pellet level, diffusion between the external surface of the pellet and the external surface of the carbon nodules is considered. At the nodule level, only diffusion inside the micropores of the carbon nodules is taken into account. It must be noted that no definite conclusion concerning the metal particles location in the pore texture can be deduced from the catalyst characterization data; since the catalysts are prepared by impregnation of a support, the particles can be deposited on the meso- or macropore surface, which corresponds to the external nodule surface, or enter the micropores. It is reasonable to think that the metal particles are at least partly dispersed on the meso- or macropore surface, the mean alloy particle sizes ranging from 3 to 6 nm. In this case, mass transfer in micropores is irrelevant. Nevertheless, the alloy particle sizes given in Table 3 are only mean values, and smaller particles could be inserted in the micropores too. Since the metal particles can be located either on the external surface of the carbon nodules or inside the micropores,

mass transfer phenomena were studied according to the two-level model described above. Note that the meaning and units of any symbol used in the discussion below are given in a list at the end of the article.

Mass transfer limitations were examined at 573 and 623 K using the data obtained at these two temperature steps. The data used at 573 K are those obtained between 12 and 17 h reaction (second step at 573 K). The presence of pore diffusion limitations in a catalyst is generally analyzed via the estimation of the Weisz modulus,[24] ϕ:

$$\Phi = \frac{r\rho L^2}{D_e C_s} \tag{6}$$

This modulus compares the observed reaction rate to the diffusion rate. The advantage of using the Weisz modulus is that each parameter is accessible to the experimenter either by measurement or by calculation; knowledge of the intrinsic reaction rate is not necessary. When $\phi \ll 1$, the pore diffusion limitation is not significant and the observed reaction rate r is equal to the intrinsic reaction rate. When $\phi \gg 1$, pore diffusion limitations modify the apparent kinetics, and r can be very different from the intrinsic reaction rate. In the classical diffusion calculation, the whole pellet is regarded as a pseudo-homogeneous medium, and one single Weisz modulus ϕ is calculated. Since carbon xerogels are modeled as a two-level system, both levels can be assimilated to a pseudo-homogeneous medium characterized by its own Weisz modulus. At the pellet level, the Weisz modulus ϕ_p is defined as:

$$\Phi_p = \frac{r_1 \rho_p L_p^2}{D_{e,p} C_{Ds,p}} \tag{7}$$

At the nodule level, Eq. 6 becomes:

$$\Phi_n = \frac{r_1 \rho_n L_n^2}{D_{e,n} C_{Ds,n}} \tag{8}$$

If both pellet and carbon nodule are considered as spheres, L_p and L_n are equal to $d_p/6$ and $d_n/6$, respectively. d_p is fixed by the sifting. Note that since the pellets are not spherical after crushing, the d_p values are probably underestimated when chosen equal to the mean between the two mesh widths, especially in the case of support X-625. Indeed, when crushed, this support smashes into flat pieces whose true thickness can be smaller than the lowest mesh width. The slab geometry would probably be more accurate, but it is not easy to estimate the slab thickness. The value taken for each catalyst is then the lowest of the two mesh widths. d_n was estimated from TEM micrographs for each xerogel support (X-525: $d_n = 100 \times 10^{-9}$ m; X-570: $d_n = 30 \times 10^{-9}$ m; X-625: $d_n = 10 \times 10^{-9}$ m). The value of d_n is not easy to determine either. Indeed, the carbon nodules are generally strongly interconnected and entangled; the error on this parameter can be large, probably about 30% high. ρ_p was obtained from mercury pycnometry measurements (Table 1: X-525-C = 400 kg m^{-3}; X-570-C = 640 kg m^{-3}; X-625-C = 1160 kg m^{-3}). ρ_n is calculated from the pellet bulk density, ρ_p, the total void volume, V_v, and the micropore volume, V_{DUB}, or from the skeletal density of the carbon material, ρ_s, and the micropore volume, V_{DUB}:

$$\rho_n = \left(\frac{1}{\rho_p} - (V_v - V_{DUB}) \right)^{-1} \tag{9}$$

$$\rho_n = \left(\frac{1}{\rho_s} + V_{DUB} \right)^{-1} \tag{10}$$

Equations 9 and 10 constitute a redundant system: V_v, V_{DUB}, ρ_s, and ρ_p are measured independently, but any of these four parameters can be calculated from the three others. Values presented in Table 1 are in good agreement with each other: whatever the calculation method and the xerogel support, ρ_n is found ranging from 1400 to 1500 kg m^{-3}. Results mentioned for ρ_n are those calculated with Eq. 10. ρ_n is the same in each catalyst because the only difference between the three xerogel supports is the nodule size (and, therefore, the size of the internodular voids corresponding to meso- and macropores), the nature, composition, and morphology of the nodules themselves remaining unchanged. The blocking of micropores by metal particles does not affect notably the nodule density.

The effective diffusivity, D_e, is the diffusivity in the pores, D, corrected by the accessible void fraction, ε, and the pore tortuosity, τ:

$$D_e = \frac{\varepsilon}{\tau} D \tag{11}$$

Moreover, the diffusivity D can be developed as a combination of both the molecular and the Knudsen diffusivities (Bosanquet formula[24]). Assuming that the tortuosity factor is at each level inversely proportional to the void fraction and using the Knudsen diffusivity equation,[24,30] Eqs. 7 and 8 can be developed as:

$$\Phi_p = \frac{r_1 \rho_p L_p^2}{C_{Ds,p}} \frac{\dfrac{1}{D_m} + \dfrac{2}{97 \times 10^{-3} w_{0,p} \sqrt{\dfrac{T}{M}}}}{\varepsilon_p^2} \tag{12}$$

$$\Phi_n = \frac{r_1 \rho_n L_n^2}{C_{Ds,n}} \frac{\dfrac{1}{D_m} + \dfrac{2}{97 \times 10^{-3} w_{0,n} \sqrt{\dfrac{T}{M}}}}{\varepsilon_n^2} \tag{13}$$

The accessible void fraction of the catalyst pellet, ε_p, and that of the catalyst nodule, ε_n, were estimated from the total void volume, V_v, the micropores volume, V_{DUB}, and the bulk density of the catalyst pellets, ρ_p. Indeed:

$$\varepsilon_p = \frac{V_v - V_{DUB}}{\dfrac{1}{\rho_p}} \tag{14}$$

$$\varepsilon_n = \frac{V_{DUB}}{\dfrac{1}{\rho_p} - (V_v - V_{DUB})} \tag{15}$$

Since the meso- or macropores volume is very different in each support, the void fraction of the catalyst pellet depends on the xerogel chosen (X-525-C: $\varepsilon_p = 0.71$; X-570-C: $\varepsilon_p = 0.53$; X-625-C: $\varepsilon_p = 0.19$). The void volume of the nodules remains constant in the case of the supports before impregnation ($\varepsilon_n = 0.35$), but due to micropores blocking, ε_n is not the same in each catalyst because the micropore volume decrease after impregnation depends on the support (X-525-C: $\varepsilon_n = 0.07$; X-570-C: $\varepsilon_n = 0.21$; X-625-C: $\varepsilon_n = 0.09$). $w_{0,p}$ represents the width of the internodular voids (meso- and macropores); in order to calculate mean values of the Weisz modulus, $w_{0,p}$ was chosen equal to the mean meso- or macropore size obtained from the pore size distribution (Figure 2a. X-525-C: $w_{0,p} = 60 \times 10^{-9}$ m; X-570-C: $w_{0,p} = 25 \times 10^{-9}$ m; X-625-C: $w_{0,p} = 8 \times 10^{-9}$ m). The width of the pores inside the nodules, $w_{0,n}$, is that of the micropores ($0 < w_{0,n} < 2 \times 10^{-9}$ m); for calculation, $w_{0,n}$ was kept equal to 1×10^{-9} m. Finally, since the reactants are diluted in large amounts of helium, the molecular diffusivity of 1,2-dichloroethane in the fluid, D_m, was considered equal to that of 1,2-dichloroethane in helium. D_m was calculated by means of the Chapman-Enskog equation[24] at 573 and 623 K: $D_m(573\text{ K}) = 3.92 \times 10^{-5}$ m^2 s^{-1}; $D_m(623\text{ K}) = 4.50 \times 10^{-5}$ m^2 s^{-1}.

The two last parameters to be estimated are the 1,2-dichloroethane concentrations at the external pellet surface, $C_{Ds,p}$, and at the external nodule surface, $C_{Ds,n}$. Let us first consider the pellet level. Since the reaction conditions were designed so as to eliminate external mass transfer limitations,[21] $C_{Ds,p}$ is equal to the CH_2Cl-CH_2Cl concentration in the gas flow, C_{Df}. The reactor is not differential strictly speaking, and $C_{Ds,p}$ was taken as the mean between the inlet and outlet concentrations, and calculated from the perfect gas law. Calculated values of ϕ_p are figured in Table 4 along with the effectiveness factor of each catalyst, η, that is, the ratio between the observed reaction rate and the intrinsic reaction rate. In each case, the intrinsic reaction rate was supposed to be that obtained for the smallest pellet size, at the corresponding temperature. In the case of catalyst X-625-C, the effectiveness factor decreases quickly when the pellet size increases (down to 0.47 (573 K) or 0.40 (623 K) when d_p increases up to 10^{-3} m). In parallel, ϕ_p increases rapidly with the pellet size, and is close to or higher than 1 in most cases. This confirms the existence of diffusional limitations in the pellet: the observed reaction rate decreases significantly when the pellet size increases, at both temperatures.

Note that diffusion limitations could also be present in catalyst X-625-Cp, especially at 623 K; the effectiveness factor of catalysts with larger pellet sizes would then possibly be overestimated, the intrinsic reaction rate being larger than that observed with the finely crushed sample. In the case of catalyst X-525-C, the effectiveness factor is equal or very close to unity, whatever the temperature or the pellet size. The Weisz modulus calculated at the pellet level ϕ_p is always much smaller than 1, which confirms that no diffusional limitations occur in this catalyst. All other parameters remaining unchanged, ϕ_p would be equal to unity, with about $d_p = 7 \times 10^{-3}$ m at 573 K. At 623 K, ϕ_p would reach unity, with $d_p = 4 \times 10^{-3}$ m. Should larger pellets be necessary to be used in a fixed bed reactor, the mean pore size could be enlarged by choosing other support synthesis conditions, that is, by decreasing the pH of the resorcinol-formaldehyde precursors solution[2,5,9]; the pore size limit is nevertheless fixed by the mechanical resistance of the pellets. Catalyst X-570-C displays an intermediate behavior; the effectiveness factor decreases (to 0.83-0.84) for the largest pellet sizes only. In parallel, the value of ϕ_p gets closer to 1.

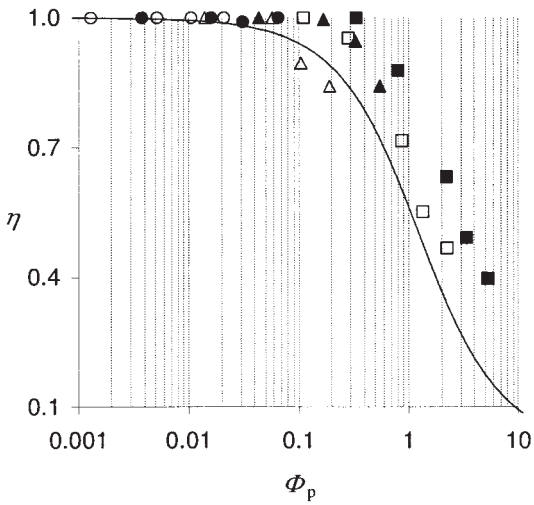

Figure 6. Effectiveness factor η as a function of the Weisz modulus at the pellet level ϕ_p at 573 K (empty symbols) and at 623 K (plain symbols).

X-525-C (● and ○), X-570-C (△ and ▲), and X-625-C (■ and □). The continuous curve represents the theoretical relationship for a first-order reaction and isothermal conditions (spherical pellet).

Considering a first-order reaction, isothermal conditions, and spherical pellets, η is correlated to ϕ_p as shown in Figure 6 (black curve).[24] The reaction conditions can be assumed to be isothermal because the reactants are diluted in helium and the enthalpy of reaction of hydrodechlorination of 1,2-dichloroethane is low[32] (~ -7 kJ mol^{-1}). Moreover, the temperature of the catalyst measured inside the reactor was not higher than the oven temperature. The values of η as a function of ϕ_p, calculated for each catalyst at 573 and 623 K, are reported on the same figure. Results are in good agreement with the theoretical curve. The largest deviations are observed for catalyst X-625-C at 623 K; globally, the experimental points are shifted upwards and/or to the right of the theoretical curve. Several factors may be taken into account in order to explain the deviations: (i) the hydrodechlorination of 1,2-dichloroethane into ethylene is not exactly first-order; the complete reaction mechanism and reaction rate expression were determined in a previous study[33]; (ii) the reactor is not totally differential, which induces errors on the reactant concentration; (iii) the intrinsic reaction rate, considered as equal to the reaction rate observed for the smallest pellet size, may be underestimated, especially at 623 K; underestimating the intrinsic reaction rate would lead to shifting up the calculated points with regard to the theoretical curve; (iv) when crushed, catalyst X-625-C can break into flat pieces instead of pellets of regular shape (spheres); considering the lowest mesh width as the pellet diameter still may overestimate the pellet characteristic dimension; this error leads to shifting the calculated points to the right of the diagram. This problem seems less important in the case of the two other xerogels, which are more friable and break into more regular fragments.

Nevertheless, the gap between the results and the theoretical curve is small enough to validate the calculation method and the hypothesis.

Let us now consider the nodule level. When no diffusional limitations are detected at the pellet level ($\phi_p \ll 1$), $C_{Ds,p} = C_{Ds,n}$ and ϕ_n can be calculated by using the same concentration value as at the upper level. When diffusion phenomena become significant ($\phi_p \geq 1$), the diffusion resistance causes a concentration profile to exist in the pellet, and the concentration at the nodule surface depends on the nodule location inside the pellet; as the distance between the pellet surface and the nodule surface increases, the reactant concentration at the nodule surface decreases. In order to check whether the reactants concentration decrease significantly affects the Weisz modulus calculation, the concentration profile must be determined. The concentration profile in the pellet is a function of the Thiele modulus,[24] φ_p, which compares the intrinsic reaction rate to the diffusion rate. The evaluation of the Thiele modulus provides then an estimation of the reactant concentration decrease at the center of the pellet; relationships between the concentration profile and the Thiele modulus are available for various operating conditions and pellet geometries.[24,27] Moreover, in the case of any n^{th} order reaction rate, one can write:

$$\Phi_p = \eta \varphi_p^2 \tag{16}$$

Diffusional limitations are certainly the most marked in catalyst X-625-C-1000; indeed, this catalyst possesses the smallest pore size, the smallest void fraction, and the largest pellet size. The Thiele modulus can be estimated from the calculated values of ϕ_p and η. For catalyst X-625-C-1000, φ_p was calculated to be 2.2 at 573 K and 3.6 at 623 K. If one refers to diagrams representing the concentration profile in spherical pellets as a function of the Thiele modulus,[24,27] the concentration of 1,2-dichloroethane in meso- or macropores at the center of the pellet decreases to 20% of the pellet surface concentration at 573 K, and to 5% at 623 K. This means that using $C_{Ds,n} = C_{Ds,p} = C_{Df}$ in the calculation of ϕ_n in the case of catalyst X-625-C-1000 leads to underestimating the Weisz modulus at the nodule level, but does not modify very much its order of magnitude. As a first approximation, the same surface concentration value was thus considered for both the pellet and the nodule level in each case. The consequences of this hypothesis should be discussed after evaluation of ϕ_n.

The calculated values of ϕ_n are given in Table 4. At the nodule level, the Weisz modulus is in each case much smaller than 1, whatever the xerogel support, the temperature, and the pellet size. Given that ϕ_n is always extremely small (from 8×10^{-9} to 1×10^{-5}), the assumption $C_{Ds,p} = C_{Ds,n}$ does not change anything; in extreme circumstances (X-625-C-1000 at 623 K: $0.05 C_{Ds,p} = C_{Ds,n}$), ϕ_n would be multiplied by 20. It is also possible to estimate the nodule size leading to diffusional limitations at that level. At 573 K, all other parameters remaining unchanged, ϕ_n would be equal to unity, with about $d_n = 0.05 \times 10^{-3}$ m to 0.2×10^{-3} m, depending on the void fraction of the nodules (0.07-0.21) and taking into account the reactant concentration decrease in the pellet due to diffusional limitations in the case of catalyst X-625-C. At 623 K, diffusional limitations would appear for d_n ranging from 0.015×10^{-3} m to 0.08×10^{-3} m. These nodule sizes are far larger than the maximum nodule size that can be obtained with carbon xerogels produced from resorcinol-formaldehyde aqueous mixtures (that is, a few micrometers). Note that the molecule size is in the order of magnitude of the micropores size; such a width represents a boundary between the Knudsen diffusion and the configurational diffusion.[25] Values of configurational diffusivity can be smaller than values of Knudsen diffusivities by several orders of magnitude. The actual diffusivity of $CH_2Cl\text{-}CH_2Cl$ could be much smaller than the one calculated by the Knudsen formula, and the obtained values of ϕ_n could be underestimated. However, since ϕ_n is extremely low in all cases, one can reasonably consider that taking the configurational diffusion into account would not lead to values of ϕ_n close to 1, except maybe in the case of micron-sized nodules.

The selectivity of the catalysts is also affected by mass transfer limitations. Table 4 shows that ethylene selectivity is close to 100% when no diffusional limitations occur (X-525-C), but can fall down to 71.8% (573 K) and 81.6% (623 K) in the case of X-625-C. This phenomenon can be explained by the fact that the hydrodechlorination of 1,2-dichloroethane into ethylene may be followed by hydrogenation of ethylene into ethane. Indeed, in the case of Pd-Ag alloys, a previous study[33] showed that the reaction mechanism includes the following steps: (i) dissociative adsorption of 1,2-dichloroethane on Ag sites with successive breakings of the two C-Cl bonds followed by (ii) desorption of ethylene and (iii) dechlorination of the silver surface by hydrogen adsorbed on Pd (production of HCl). As Pd can store hydrogen by dissociative chemisorption, Pd present at the alloy surface supplies hydrogen atoms for the regeneration of the chlorinated Ag surface into metallic Ag. But hydrogen adsorbed on Pd may also cause ethylene hydrogenation. This reaction is favored by the presence of large amounts of Pd at the surface of the Pd-Ag alloy particles. Therefore, the selectivity of the Pd-Ag catalysts depends on the surface composition of the alloy, but also on the residence time of ethylene inside the catalyst.

The conversion of ethylene into ethane is favored when the diffusional limitations prevent ethylene from leaving the catalyst pellet. Considering the reaction rate equation,[33] one can assume, as a first approximation, that the hydrodechlorination of 1,2-dichloroethane into ethylene is first-order with regard to 1,2-dichloroethane, and that the hydrogenation of the ethylene step is first-order with regard to both ethylene and hydrogen. For all the catalysts operating at 573 and 623 K, the concentration of hydrogen is about ten times larger (or more) than that of ethylene. This enables us to consider the hydrogenation reaction as pseudo first-order with regard to ethylene. For sample X-625-Cp, considered as free of limitations, one can write that:

$$\rho_p r_1 = k_1 C_{Ds,p} = k_1 C_{Df} \tag{17}$$

$$\rho_p r_2 = k_2 C_{Hs,p} C_{Es,p} = k_2 C_{Hf} C_{Ef} = k_2' C_{Ef} \quad \text{with} \quad k_2 C_{Hf} = k_2' \tag{18}$$

If the volume change during reaction is neglected, the selectivity in chemical regime, S_{CHEM}, defined as the ratio between the rate of concentration variation of ethylene and that of 1,2-dichloroethane at an effectiveness factor approaching unity, is[24]:

Table 5. Data Related to Catalyst X-625-Cp

T (K)	r_2 (mmol kg^{-1} s^{-1})	C_{Df} (mmol m^{-3})	C_{Ef} (mmol m^{-3})
573	0.34	1485	101
623	0.69	1215	247

$$S_{CHEM} = -\frac{dC_{Ef}}{dC_{Df}} = 1 - \frac{r_2}{r_1} \tag{19}$$

For catalyst X-625-Cp, r_1 and r_2 were obtained from measurements at the reactor outlet (Tables 4 and 5): r_1 (573 K) = 7.6 mmol kg_{cat}^{-1} s^{-1}; r_1 (623 K) = 19.6 mmol kg_{cat}^{-1} s^{-1}; r_2 (573 K) = 0.34 mmol kg_{cat}^{-1} s^{-1}; r_2 (623 K) = 0.69 mmol kg_{cat}^{-1} s^{-1}. From Eq. 19, one obtains S_{CHEM} (573 K) = 96% and S_{CHEM} (623 K) = 97%, which is in good agreement with selectivity values obtained for X-625-Cp (Figure 5b). For the case where the porous catalyst operates at a low effectiveness factor ($\phi_p > 3$), the selectivity in strong diffusional control, S_{DIFF}, becomes[24]:

$$S_{DIFF} = -\frac{dC_{Ef}}{dC_{Df}} = \frac{1}{1 + \sqrt{\frac{k_2'}{k_1}}} - \sqrt{\frac{k_2'}{k_1}}\frac{C_{Ef}}{C_{Df}} = \frac{1}{1 + \sqrt{\frac{r_2 C_{Df}}{r_1 C_{Ef}}}} - \sqrt{\frac{r_2 C_{Df}}{r_1 C_{Ef}}}\frac{C_{Ef}}{C_{Df}} \tag{20}$$

where r_1 and r_2 remain the intrinsic reaction rates, that is, the values obtained for catalyst X-625-Cp. C_{Ef} and C_{Df} were obtained from measurements at the reactor outlet, the concentrations being taken equal to the mean between the inlet and the outlet of the reactor (Table 5) : C_{Df}(573 K) = 1485 mmol m^{-3}; C_{Df}(623 K) = 1215 mmol m^{-3}; C_{Ef}(573 K) = 101 mmol m^{-3}; C_{Ef}(623 K) = 247 mmol m^{-3}. From Eq. 20, one obtains S_{DIFF} (573 K) = 50% and S_{DIFF} (623 K) = 62%. These values are lower than those obtained experimentally for X-625-C-1000 (573 K: 71.8%; 623 K: 81.6%), which indicates that the catalyst behavior is probably intermediate between strong and no pore diffusion. At 573 K, for sample X-625-C-1000, we calculated $\phi_p = 2.2$ (Table 4), which is indeed lower than the limit for strong pore diffusion[24] ($\phi_p > 3$). At 623 K, however, the value obtained for the Weisz modulus was $\phi_p = 5.3$. This indicates that the Weisz modulus is slightly overestimated, which could confirm that the deviation from the theoretical curve $\eta = f(\phi_p)$ is due to a slight overestimation of the pellet characteristic dimension.

Pd-Ag catalysts supported on activated carbon NC45 were not discussed yet. The main problem is that the support is extremely heterogeneous, the meso- and macropore size distribution ranging from 10×10^{-9} to 4×10^{-6} m. It is then impossible to define one single pertinent pore size in this range from textural characterization data. The two-level model used for the xerogels support is certainly not applicable either. In fact, the activated carbon support should better be regarded as homogeneous porous zones separated by channels large enough to be without effect on mass transfer; the pseudo-homogeneous pellet concept would then not apply to the whole pellet, but to the small zones separated by large pores or cracks.[34] Therefore, the difficulty consists in determining the characteristic size of these homogeneous zones. Table 4 shows that results obtained with catalyst NC45-C are identical in the case of the two largest pellet sizes (NC45-C-1000 and NC45-C-710: conversion = 5.6% at 573 K and 18.0% at 623 K). This implies that the characteristic size of the catalyst is not modified by crushing if the pellet size is not lower; large pellets certainly break preferentially along large pores or cracks that play no role in mass transfer limitations. The conversion increases slightly with NC45-C-500 (573 K: 6.3%; 623 K: 20.0%) and reaches its maximal values with NC-45-C-250 (573 K: 8.7%; 623 K: 26.8%). This suggests that the homogeneous zones to be considered are probably 0.7-0.8 $\times 10^{-3}$ m wide. Since the effectiveness factors of NC45-C-1000 and NC45-C-710 range from 0.64 to 0.68 at both temperatures, Figure 6 indicates that the values of the Weisz modulus related to the homogeneous zones are contained between 1.3 and 1.0. If one considers that the homogeneous zones of the support are spherical and 0.75×10^{-3} m in diameter, the pore size leading to the observed values of the effectiveness factor should be lower than about 10×10^{-9} m. This is in good agreement with the assumption that all the macroporosity has to be excluded from the homogeneous zone.

The four catalysts obtained with various supports and displaying pellet size small enough to consider that diffusional limitations are eliminated do not lead to the same catalytic activity. Table 4 shows that the conversion obtained with catalysts considered as free of limitations varies from 8.7% to 21.3% at 573 K, and from 26.8% to 55% at 623 K. This variation is not related to the actual metals contents. The lowest conversion is obtained with the catalyst supported on activated charcoal. This can be explained by the alloy particle size; indeed, the particles are larger than in the case of xerogel supported catalysts (5-6 nm instead of 3-4 nm). In the case of xerogel supported catalysts, the highest conversion was obtained with X-570-C, whatever the temperature: 21.3% at 573 K and 55.0% at 623 K. For comparison, X-525-C and X-625-C display conversions equal to 12.1 and 12.5% at 573 K, and equal to 34.3 and 31.7% at 623 K, respectively. This conversion difference cannot be explained by alloy particle size variations: the alloy particle size is almost identical in the three catalysts. The only possible explanation is that the accessible alloy surface is different. It was noticed that the specific surface area of catalysts X-525-C and X-625-C decreased more during metal deposition than that of X-570-C (ΔS_{BET} = 515 and 470 $\times 10^3$ m^2 kg^{-1} instead of $\Delta S_{BET} = 250 \times 10^3$ m^2 kg^{-1}, respectively). This result indicates that a larger part of the micropores is blocked by metal particles after impregnation in catalysts X-525-C and X-625-C. It is then possible that some metal particles are only accessible from one side, or completely confined in micropores blocked by larger particles.

The catalytic results and specific surface areas measured show that this phenomenon is less marked for X-570-C, whose support displays the largest mesopores volume. This could indicate that micropores tend to remain free when the mesopores surface increases. The beneficial effect of mesopores in carbon supports on the metal dispersion was previously observed. For example, it was shown that developing the mesopores surface of the support could enhance the accessible surface of platinum particles deposited on activated charcoal.[35] But since the dispersion measurements were not coupled with particle size evaluation in the cited study, the dispersion en-

hancement can be due either to the decrease of the particle size or to the increase of the particles accessibility.

Conclusion

Hydrodechlorination of 1,2-dichloroethane into ethylene was chosen as a test reaction in order to study mass transfer in carbon xerogel supported catalysts. Results show that diffusional limitations can be completely avoided by choosing an appropriate pore size range, which is made possible by the pore texture flexibility of carbon supports issued from drying and pyrolysis of resorcinol-formaldehyde aqueous gels. Indeed, a support with small mesopores (pores smaller than 10×10^{-9} m) leads to diffusional limitations, whatever the temperature chosen, as soon as the pellet size is larger than 0.250×10^{-3} m. On the contrary, in the case of a macroporous support (pore size range = 60 to 80 $\times$ 10^{-9} m), the 1,2-dichloroethane conversion, ethylene selectivity, and reaction rate are completely independent from the pellet size up to about 4×10^{-3} m (623 K) and 7×10^{-3} m (573 K). Should the reaction rate be higher, the pore size could be chosen larger than 80×10^{-9} m by decreasing the initial pH of the resorcinol-formaldehyde aqueous solution. Note that when the pore size is larger than 100×10^{-9} m, the Knudsen diffusion is not significant and the diffusion coefficient is not related to the pore size anymore. The only textural parameter that plays a role in diffusion is the void fraction of the support (assuming that the tortuosity factor is inversely proportional to the void fraction). Enlarging the pores above 100×10^{-9} m would not improve the catalyst performance.

Active charcoals, which are widely used in heterogeneous catalysis, are generally microporous with low meso- and macropore volume. This often induces diffusional limitations and a decrease of the catalyst performance. Their texture strongly depends on the raw material chosen, and cannot be easily modified by thermal or chemical treatments. Since the production of carbon xerogels with the tailored texture method is very simple, active charcoals could be replaced by xerogels with a pore texture adapted to the considered reaction. The only limitation to pore size concerns the mechanical properties of the pellets: the xerogel support becomes friable when the pore volume and pore size are too large (>250 nm). Nevertheless, the pore size and pore volume range accessible by the sol-gel process and suitable to catalysts supports is very wide, which makes carbon xerogels very attractive as an alternative to classical active charcoal supports.

Acknowledgments

The authors thank the Belgian Fonds National de la Recherche Scientifique, the Région Wallonne - Direction Générale des Technologies, de la Recherche et de l'Energie, the Ministère de la Communauté française - Direction de la Recherche scientifique, and the Fonds de Bay for their financial support. BV and JFC thank the FNRS (Belgium) for a research fellowship. The authors are also grateful to Mr. S. G. Apter from the Department of Chemistry of the University of Liverpool for the ICP-AES measurements. The authors also acknowledge the involvement of their laboratory in the Network of Excellence FAME of the European Union sixth framework program.

Notation

C = reactant concentration (mmol m^{-3})
d = diameter of the considered porous object (m)
D = diffusivity in the pores of the porous object (m^2 s^{-1})
D_e = effective diffusion coefficient (m^2 s^{-1})
D_K = Knudsen diffusion coefficient (m^2 s^{-1})
D_m = molecular diffusion coefficient (m^2 s^{-1})
k_1 = CH_2Cl-CH_2Cl hydrodechlorination reaction rate constant (s^{-1})
k_2 = CH_2=CH_2 hydrogenation reaction rate constant (m^3 $mmol^{-1}$ s^{-1})
L = ratio between the volume and the external surface of the porous object considered (m)
M = molar weight of 1,2-dichloroethane (98.9596×10^{-6} kg $mmol^{-1}$)
r = observed reaction rate (mmol kg_{cat}^{-1} s^{-1})
S_{CHEM} = selectivity in CH_2=CH_2 in chemical regime (%)
S_{DIFF} = selectivity in CH_2=CH_2 in diffusional regime (%)
T = temperature (K)
V_{DUB} = volume of pores smaller than 2×10^{-9} m (m^3 kg^{-1})
V_v = total void volume (m^3 kg^{-1})
w_0 = mean pores width (m)
$w_{0,max}$ = maximum pore width (m)

Greek letters

ε = void fraction
η = catalyst effectiveness factor
ρ = bulk density of the considered carbon object (kg m^{-3})
ρ_s = skeletal density (that is, apparent density) of the carbon support (kg m^{-3})
τ = tortuosity factor
φ = Thiele modulus
ϕ = Weisz modulus

Subscripts

n = at the nodule level
p = at the pellet level
s = at the surface of the porous object considered
f = in the gas flow
D = dichloroethane
E = ethylene
H = hydrogen
1 = related to the hydrodechlorination of CH_2Cl-CH_2Cl into CH_2=CH_2
2 = related to the hydrogenation of CH_2=CH_2 into CH_3-CH_3

Literature Cited

1. Pekala RW. Organic aerogels from the polycondensation of resorcinol with formaldehyde. *J Mater Sci.* 1989;24:3221-3227.
2. Al-Muhtaseb SA, Ritter JA. Preparation and properties of resorcinol-formaldehyde organic and carbon gels. *Adv Mater.* 2003;15:101-114.
3. Moreno-Castilla C, Maldonado-Hódar FJ. Carbon aerogels for catalysis applications: an overview. *Carbon.* 2005;43:455-465.
4. Pirard JP, Pirard R, Job N. Patent WO 03/026048 A1; 2003.
5. Job N, Pirard R, Marien J, Pirard JP. Porous carbon xerogels with texture tailored by pH control during sol-gel process. *Carbon.* 2003; 42:619-628.
6. Job N, Pirard R, Marien J, Pirard JP. Synthesis of transition metal-doped carbon xerogels by solubilization of metal salts in resorcinol-formaldehyde aqueous solution. *Carbon.* 2004;42:3217-3227.
7. Léonard A, Job N, Blacher S, Pirard JP, Crine M, Jomaa W. Suitability of convective air drying for the production of porous resorcinol-formaldehyde xerogels. *Carbon.* 2005;43:1808-1811.
8. Job N, Panariello F, Marien J, Crine M, Pirard JP, Léonard A. Synthesis optimization of organic xerogels produced from convective air-drying of resorcinol-formaldehyde gels. *J Non-Cryst Solids.* 2006; 352:24-34.
9. Job N, Théry A, Pirard R, Marien J, Kocon L, Rouzaud JN, Béguin F, Pirard JP. Carbon aerogels, cryogels and xerogels: influence of the drying method on the textural properties of porous carbon materials. *Carbon.* 2005;43:2481-2494.
10. Maldonado-Hódar FJ, Ferro-Garcia MA, Rivera-Utrilla J, Moreno-Castilla C. Synthesis and textural characterization of organic aerogels, transition-metal-containing aerogels and their carbonized derivatives. *Carbon.* 1999;37:1199-1205.

11. Byrne JF, Marsh H. "Introductory overview," *Porosity in Carbons*, Patrick JW, ed. London: Wiley; 1995:1-66.
12. Job N, Heinrichs B, Ferauche F, Noville F, Marien J, Pirard JP. Hydrodechlorination of 1,2-dichloroethane on Pd-Ag catalysts supported on tailored texture carbon xerogels. *Catal Today.* 2005;102-103:234-241.
13. Heinrichs B, Noville F, Schoebrechts JP, Pirard JP. Palladium–silver sol–gel catalysts for selective hydrodechlorination of 1,2-dichloroethane into ethylene: IV. Deactivation mechanism and regeneration. *J Catal.* 2003;220:215-225.
14. Lecloux AJ. "Texture of catalysts," *Catalysis Science and Technology*, Anderson JR, Boudart M, eds. Berlin: Springer, Vol. 2, 1981:171-230.
15. Alié C, Pirard R, Lecloux AJ, Pirard JP. Preparation of low density xerogels through additives to TEOS-based alcogels. *J Non-Cryst Solids.* 1999;246:216-228.
16. Washburn EW. Note on a method of determining distribution of pore sizes in a porous material. *Proc Nat Acad Sci.* 1921;7:115-116.
17. Pirard R, Heinrichs B, Pirard JP. "Mercury porosimetry applied to low density xerogels," *Characterization of Porous Solids IV*, McEnaney B, Mays TJ, Rouquerol J, Rodríguez-Reineso F, Sing KSW, Unger KK, eds. Cambridge: The Royal Society of Chemistry; 1997:460-466.
18. Anderson JR. *Structure of Metallic Catalysts*. London: Academic Press; 1975.
19. Bergeret G, Gallezot P. "Particle size and dispersion measurement," *Handbook of Heterogeneous Catalysis, Vol. 2*, Ertl G, Knözinger H, Weitkamp J, eds. Weinheim: Wiley-VCH; 1997:439-464.
20. Heinrichs B, Noville F, Schoebrechts JP, Pirard JP. Palladium–silver sol–gel catalysts for selective hydrodechlorination of 1,2-dichloroethane into ethylene: II. Surface composition of alloy particles. *J Catal.* 2000;192:108-118.
21. Heinrichs B, Schoebrechts JP, Pirard JP. Mass transfer in low-density xerogel catalysts. *AIChE J.* 2001;47:1866-1873.
22. Sinfelt JH. *Bimetallic Catalysts—Discoveries, Concepts, and Applications*. New York: Wiley; 1983.
23. Soma-Noto Y, Sachtler WMH. Infrared spectra of carbon monoxide adsorbed on supported palladium and palladium-silver alloys. *J Catal.* 1974;32:315-324.
24. Satterfield CN. *Mass Transfer in Heterogeneous Catalysis*. Cambridge, MA: MIT Press; 1970.
25. Weisz PB. Zeolites—new horizons in catalysis. *Chem Tech* 1973;3:498–505.
26. Carberry JJ. "Physico-chemical aspect of mass and heat transfer in heterogeneous catalysis," *Catalysis: Science and Technology, Vol. 8*, Anderson JR, Boudart M, eds. Berlin: Springer; 1987:131.
27. Froment GF, Bischoff KB. *Chemical Reactor Analysis and Design*, 2nd ed. New York: Wiley; 1990.
28. Villermaux J. *Génie de la reaction chimique – Conception et Fonctionnement des Réacteurs*. Paris: Lavoisier; 1993.
29. Emig G, Dittmeyer R. "Simultaneous heat and mass transfer and chemical reaction," *Handbook of Heterogeneous Catalysis, Vol. 3*, Ertl G, Knözinger H, Weitkamp J, eds. Weinheim, Germany: Wiley-VCH; 1997:1209-1252.
30. Kapteijn F, Moulijn JA. "Laboratory catalytic reactors: aspects of catalyst testing," *Handbook of Heterogeneous Catalysis, Vol. 3*, Ertl G, Knözinger H, Weitkamp J, eds. Weinheim, Germany: Wiley-VCH; 1997:1359-1376.
31. Alié C, Ferauche F, Léonard A, Lambert S, Tcherkassova N, Heinrichs B, Crine M, Marchot P, Loukine E, Pirard JP. Pd-Ag/SiO2 xerogel catalyst forming by impregnation on alumina foams. *Chem Eng J.* 2006;117:13-22.
32. Lacher JR, Amador A, Park JD. Reaction heats of organic compounds, Part 5—Heats of hydrogenation of dichloromethane, 1,1- and 1,2-dichloroethane and 1,2-dichloropropane. *Trans Farad Soc.* 1967;63:1608-1611.
33. Heinrichs B, Schoebrechts JP, Pirard JP. Palladium–silver sol–sel catalysts for selective hydrodechlorination of 1,2-dichloroethane into ethylene: III. Kinetics and reaction mechanism. *J Catal.* 2001;200:309-320.
34. McKenna TF, Cokljat D, Spitz R, Schweich D. Modelling of heat and mass transfer during the polymerisation of olefins on heterogeneous Ziegler catalysts. *Catal Today.* 1999;48:101-108.
35. Prado-Burguete C, Linares-Solano A, Rodríguez-Reinoso A, Salinas-Martínez de Lecea C. Effect of carbon support and mean Pt particle size on hydrogen chemisorption by carbon-supported Pt catalysts. *J Catal.* 1991;128:397-404.

Manuscript received Oct. 1, 2005, and revision received Mar. 8, 2006.